Available online at www.sciencedirect.com

ScienceDirect

journal homepage: www.elsevier.com/locate/he

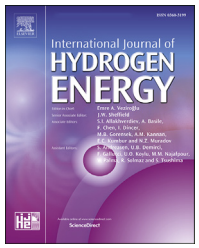

Thermodynamic and kinetic properties of calcium hydride

Sruthy Balakrishnan, Terry D. Humphries, Mark Paskevicius, Craig E. Buckley*

Physics and Astronomy, School of Electrical Engineering, Computing and Mathematical Sciences, Curtin University, GPO Box U1987, Perth, WA, 6845, Australia

HIGHLIGHTS

- The thermodynamics for hydrogen desorption of calcium hydride were determined.
- This is the first study in over 60 years to determine the thermal properties.
- The kinetics of hydrogen release were measured using the Kissinger method.
- The melting point of CaH_2 was measured under a hydrogen atmosphere.
- A literature review of previous thermodynamic studies on CaH_2 is included.

ARTICLE INFO

Article history:
Received 1 March 2023
Received in revised form
3 April 2023
Accepted 7 April 2023
Available online 5 May 2023

Keywords:
Metal hydride
Hydrogen storage
Activation energy
Kissinger plot
Thermal analysis
Thermodynamics

ABSTRACT

Calcium hydride has shown great potential as a hydrogen storage material and as a thermochemical energy storage material. To date, its high operating temperature (above 800 °C) has not only hindered its opportunity for technological application but also prevented detailed determination of its thermodynamics of hydrogen sorption. In addition, calcium metal suffers from high volatility, high corrosivity from Ca (and CaH_2), slow kinetics of hydrogen sorption, and the solubility of Ca in CaH_2. In this work, a literature review of the wide-ranging thermodynamic properties of CaH_2 is provided along with a detailed experimental investigation into the thermodynamic properties of molten and solid CaH_2. The thermodynamic values of hydrogen release from both molten and solid CaH_2 were determined as ΔH_{des} (molten CaH_2) = 216 ± 10 kJ $mol^{-1}.H_2$, ΔS_{des} (molten CaH_2) = 177 ± 9 J K^{-1} $mol^{-1}.H_2$, which equates to a 1 bar hydrogen equilibrium temperature for molten CaH_2 of 947 ± 65 °C. Similarly, in the solid-state: ΔH_{des} (solid CaH_2)- = 172 ± 12 kJ $mol^{-1}.H_2$, ΔS_{des} (solid CaH_2) = 144 ± 10 J K^{-1} $mol^{-1}.H_2$. Moreover, the activation energy of hydrogen release from CaH_2 was also calculated using DSC analysis as E_a- = 203 ± 12 kJ mol^{-1}. This study provides the first thermodynamics for the Ca–H system in over 60 years, providing more accurate data on this emerging energy storage material.

* *Corresponding author.*
E-mail address: terry_humphries81@hotmail.com (T.D. Humphries).

https://doi.org/10.1016/j.ijhydene.2023.04.088

Introduction

Calcium hydride was first reported to exist in 1891 by Clemens A. Winkler [1], who heated lime (CaO) and Mg together under an H_2 atmosphere to form "CaH". In 1893, Henri Moissan produced CaH_2 from Ca and steam [1]. Since then, CaH_2 has been produced on an industrial scale and utilised in many practical purposes including as a source of hydrogen, a reducing agent, catalyst, solvent purification agent, condensing and drying agent, and even in nuclear reactors [1,2]. In earlier times, CaH_2 was called Hydrolith as it was known to react with water to release hydrogen [3]. Today, CaH_2 remains an effective source of hydrogen, and its high operating temperature at low pressures (1100–1400 °C at 1–5 bar), energy storage density for hydrogen sorption (4939 kJ kg^{-1}) and reversible hydrogen storage property makes it attractive as a high-temperature thermochemical battery material [4,5]. The general properties of both Ca and CaH_2 are listed in Table 1.

Peterson and Fattore first reported the calcium-calcium hydride phase diagram in 1961 (Fig. 1) [20]. The phase diagram aids in understanding the allotropic transitions, and the relationship between liquid and solid phases of Ca and CaH_2 as a function of hydrogen content and temperature. The phase diagram is similar to the barium–barium hydride system except for the additional complexity arising from the allotropy of calcium [2]. A polymorphic crystal structure transition from *fcc* to *bcc* (α-Ca to β-Ca) is observed in pure Ca metal at 448 ± 2 °C on heating and 442 ± 2 °C on cooling. An intermediate *hcp* phase of Ca, γ-Ca, may exist in this temperature range depending on the hydrogen impurities present in the calcium. CaH_2 undergoes a polymorphic transition from orthorhombic (*Pnma*) to cubic ($Fm\bar{3}m$) (α-CaH_2 to β-CaH_2) at 780 °C [21]. Solid solubility of CaH_2 in Ca is observed and reaches a maximum of 24 mol% at the peritectic temperature of 890 °C [20]. Above 842 °C, beyond the melting point of Ca, liquid Ca exists with CaH_2. Unfortunately, no data is available for this system above 980 °C.

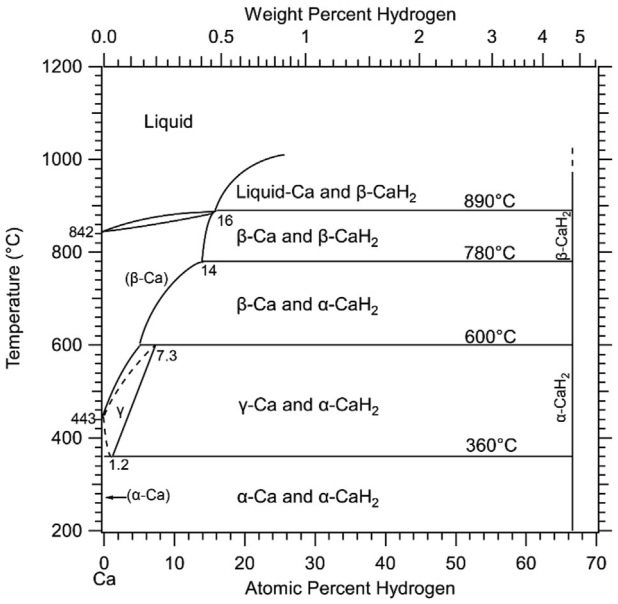

Fig. 1 – Phase diagram for the calcium-calcium hydride system. Adapted from Ref. [1].

Several authors have studied the Ca–CaH_2 system by conducting hydrogen desorption pressure composition isotherm

Table 1 – The general properties of the Ca and CaH_2 system [6–9].

Physical Properties	Ca	CaH_2	Comments
Appearance	Silvery white	White to grey	White when pure CaH_2
Crystal system	Face centred cubic ($Fm\bar{3}m$)	Orthorhombic (*Pnma*)	At room temperature
Molar mass (g.mol^{-1})	40.08	42.10	
Melting point (°C)	839–852	816–1000	Depending on the purity of both Ca and CaH_2
Boiling point (°C)	1484	N/A	
Density (g.cm^{-3} at 25 °C)	1.54	1.7	
Density (g.cm^{-3} at X °C)	1.378	–	X = 842 °C (liquid)
	1.319	–	X = 1100 °C (liquid)
Thermal conductivity (W.cm^{-1}. °C^{-1} at 27 °C)	2.00	3.1	
Heat capacity at 25 °C (J mol^{-1}.°C^{-1})	25.9	41.0	
Heat capacity at X °C (J.mol^{-1}.°C^{-1})	35	75	X = 1000 °C (liquid)
Specific heat capacity at 25 °C (J kg^{-1}.°C^{-1})	647	974	
Specific heat capacity at X °C (J.kg^{-1}.°C^{-1})	873	1782	X = 1000 °C (liquid)
Hydrogen desorption enthalpy (kJ.mol^{-1} H_2)	–	~ 207.7	Different values reported by various investigators [1,10–19]
Theoretical hydrogen storage capacity (wt% H_2)	–	4.79	
Practical hydrogen storage capacity (wt% H_2)	–	~ 2.4	
1 bar hydrogen equilibrium temperature (°C)	–	~ 990	Varies from 950 to 1100 °C
Theoretical gravimetric energy density for hydrogen sorption (kJ.kg^{-1})	–	4934	
Practical gravimetric energy density for hydrogen sorption (kJ.kg^{-1})	–	2472	
Theoretical volumetric energy density for hydrogen sorption (kJ.L^{-1})	–	6508	

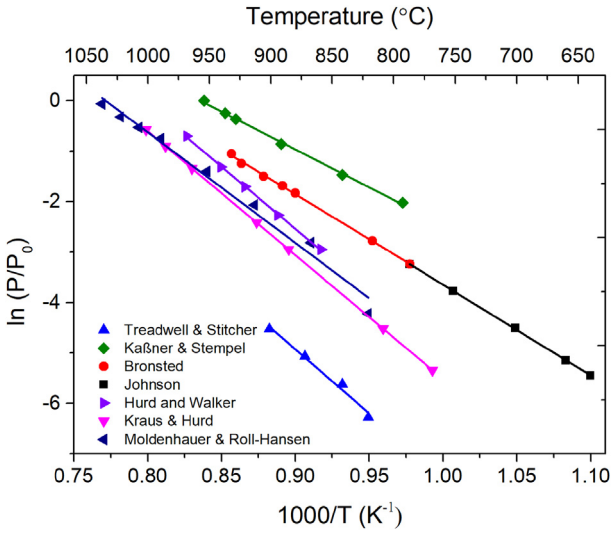

Fig. 2 – van't Hoff plot for the hydrogen desorption from CaH_2 from all previous studies [1,10–19].

(PCI) experiments. The hydrogen equilibrium pressure at corresponding temperatures for the CaH_2 system from the seven known studies has been plotted as a van't Hoff plot in Fig. 2 [10–12,15–17,19]. It is noted that the thermodynamics for the desorption of hydrogen from the CaH_2 have not been studied since 1953. All reported thermodynamic data published in the literature from 1913 to 1953, are tabulated in Table 2.

It is important to highlight that the experimental determination of thermodynamic parameters using PCI measurements (and van't Hoff plots) relies on accurate measurement of hydrogen pressure at given temperatures. In addition, each recorded pressure should be at thermodynamic equilibrium, where kinetic factors have been completely eliminated. Most importantly, the hydrogen equilibrium pressure recorded at any particular temperature will be a function of the thermodynamics of the particular chemical reaction involving hydrogen sorption. For example, based on the phase diagram (Fig. 1) there are a number of different chemical reactions that can take place, based on the temperature. For instance, at 700 °C, the decomposition of solid $\alpha - CaH_2$ will release hydrogen gas to form solid $\beta - Ca$, according to:

$$\alpha - CaH_2(s) \rightleftharpoons \beta - Ca(s) + H_2(g) \quad (1)$$

The thermodynamics of reaction will be different at other temperatures when other allotropes or phases are present. For instance, at 810 °C, $\beta - CaH_2$ is the stable crystalline polymorph of CaH_2, which will also release hydrogen to form solid $\beta - Ca$, according to:

$$\beta - CaH_2(s) \rightleftharpoons \beta - Ca(s) + H_2(g) \quad (2)$$

Therefore, the thermodynamics of reaction at 810 °C will be different to the thermodynamics of reaction at 700 °C because different reactions are occurring. This is also the case above the melting point for calcium. For instance, at 910 °C, solid $\beta - CaH_2$ will decompose to release hydrogen gas to form liquid calcium metal.

$$\beta - CaH_2(s) \rightleftharpoons Ca(l) + H_2(g) \quad (3)$$

In addition to the complexities outlined above for different structural polymorphs of both calcium and calcium hydride, along with liquid and solid phases, there is also another consideration with the fact that the phase diagram (Fig. 1) outlines certain regions (such as the solid $\beta - Ca$ region from 443 to 842 °C) where hydrogen is soluble within the metallic Ca phase without the formation of CaH_2. There is also hydrogen solubility within liquid Ca metal above this temperature range, along with CaH_2 solubility within the liquid Ca metal.

Thus, the PCI measurements of hydrogen pressure from the Ca–H system must consider the different reaction pathways that exist at different temperatures to adequately measure the correct reaction thermodynamics. Due to the time period of many of the studies investigating the thermodynamics of the Ca–H system (all are pre-1953), many have not considered these constraints, or have been working with limited knowledge of the phase diagram.

The main differences in the results and conclusions of individual investigators, as shown in Table 2, may be due to the different types of hydrogen equilibrium reactions that could exist in the CaH_2 system along with issues with the kinetics of hydrogen sorption. The four types of thermodynamic equilibrium explained in the literature, so far, can be listed as shown below:

(a) Type 1 equilibrium

The first type of equilibrium was reported in four studies by Brønsted (1914), Kraus and Hurd (1923), Remy-Cennete (1929),

Table 2 – The thermodynamic properties for the hydrogen desorption of CaH_2 from the literature [1,10–19]. The reaction enthalpy (ΔH_{des}), entropy (ΔS_{des}), and the calculated temperature where the hydrogen equilibrium pressure is 1 bar (T_{des}) are listed.

Investigator	Year	T range (°C)	ΔH_{des} (kJ.mol^{-1} H_2)	ΔS_{des} (J.K^{-1}.mol^{-1} H_2)	T_{des} (°C at 1 bar)
Moldenhauer and Roll-Hansen	1913	780–1027	182	141	1023
Bronsted	1914	641–747	197	155	997
Kraus and Hurd	1923	734–985	204	158	1017
Kaßner and Stempel	1929	755–920	123	103	926
Remy - Cennete	1929	815–970	214	N/A	N/A
Hurd and Walker	1931	816–936	205	164	977
Johnson et al.	1939	636–894	150	119	987
Treadwell and Stitcher	1953	780-860	211	149	1143

and Hurd and Walker (1931), who reported the hydrogen decomposition reaction occurs in one step, as shown in equation (4) [1,12,16,19]. This equilibrium is represented by the reaction between CaH_2, Ca and H_2, where the equilibrium hydrogen pressure is independent of solid solutions, which are not considered. All these four studies attempted to confine the calcium/calcium hydride, e.g., inside hydrogen-permeable iron tubes closed by a plug, to prevent evaporation of volatile calcium at elevated temperatures.

$$CaH_2 \rightleftharpoons Ca + H_2(g) \quad (4)$$

(b) Type 2 equilibrium

Type 2 equilibrium was reported by four studies published by Moldenhauer and Roll-Hansen (1913), Ephriam and Michel (1921), Hüttig and Brodkorb (1926), and Kaßner and Stempel (1929) [1,13–15,17]. Each determined that hydrogen release occurs in two steps, as shown in equations (5) and (6), where at equilibrium the material contains four phases, CaH_2, CaH, Ca, and H_2, and the equilibrium H_2 pressure is independent of solid solutions, which are not considered. Hüttig and Brodkorb reported a steady increase in hydrogen pressure when the system was kept at a constant temperature [13]. Moldenhauer and Roll-Hansen believed that they proved the existence of CaH [17]. In the experiments, a material with one half the usual amount of hydrogen present in CaH_2 was used, and as such the pressure measured during desorption only reached a value of one half the normal magnitude. They also stated that CaH_2 is non-volatile and that CaH is very volatile. Even though the opinions of various investigators vary concerning the reaction for the dissociation of CaH_2, they all agree that molecular hydrogen constitutes the gaseous product.

$$CaH_2 \rightleftharpoons CaH + \tfrac{1}{2} H_2(g) \quad (5)$$

$$CaH \rightleftharpoons Ca + \tfrac{1}{2} H_2(g) \quad (6)$$

(c) Type 3 equilibrium

Ephriam and Michel (1921), Hüttig and Brodkorb (1926), Hurd and Walker (1931), and Stubbs (1931) also discussed a third type of equilibrium that consists of CaH_2 and metallic Ca, which can form a series of solid solutions, where the hydrogen dissociation pressure is dependent on the composition of the condensed mixture phase [12–14]. The condensed mixture phase had a composition of CaH_2.2Ca and may vary as a function of decomposition.

(d) Type 4 equilibrium

Johnson et al. (1939) and Treadwell and Sticher (1953) reported the fourth type of equilibrium which is similar to the third type, but the dissociation pressure depends on the composition of condensed phases below 20–25% and above 90–95% CaH_2 [10,11]. Between these limits (25–90%), the hydrogen dissociation pressure is independent of the composition of the mixture of condensed phases. It should be noted that this interpretation also matches what we now know from the Ca–H phase diagram (Fig. 1). Treadwell and Sticher concluded that the condensed mixture contains a solution of calcium in calcium hydride, nCa.CaH_2 [11].

The disagreement in thermodynamics and the interpretation of results between studies, as shown in Table 2, may be due to differences in their experimental procedures. This includes the purity of both Ca and CaH_2, mode of preparation, apparatus, the form of the reactants, the difference in melting point of Ca and CaH_2, surface area, allotropic forms of Ca and CaH_2, the solubility of Ca and CaH_2 and vice versa, as explained in the previous section in the phase diagram. Also, the hydrogen sorption reactions may be further inhibited due to the presence of surface films, poor kinetics, different step sizes in PCI's, not reaching the thermodynamic equilibrium plateau during hydrogen release, and CaH_2 phase compositional variations. For the studies using open sample cells inside reactors, volatile solid products may have evaporated and deposited in the cooler parts, which could also reabsorb H_2, reducing the equilibrium pressure. Also, some studies used quartz reactors, which may have reacted with calcium hydride at high temperatures to release hydrogen [7]. These potential problems would affect the measured equilibrium pressure, and thus the measured thermodynamics. For optimal results, the sample cell should be closed to Ca and CaH_2 evaporation but be permeable to hydrogen. This is typically undertaken using sealed iron (Fe) vessels to contain reactants within a larger reactor, due to its high hydrogen gas permeability at high temperature [10].

Little research has been conducted on the Ca–H system since 1960, especially on thermodynamics and kinetics. This may be due to the extreme temperature required to achieve reasonable hydrogen gas equilibrium pressures, along with the corrosive nature and high vapour pressure of calcium. Therefore, in this study, the kinetic and thermodynamic properties of CaH_2 are experimentally re-investigated and reported separately for both solid and molten CaH_2 by undertaking PCI measurements across different temperature regimes.

Experimental methods

Calcium hydride (CaH_2, Sigma Aldrich, >95% purity), was stored and manipulated inside an argon filled MBraun Unilab glovebox to limit oxygen (<1 ppm) and water (<1 ppm) contamination. CaH_2 was ball-milled using an Across International Planetary Ball mill (PQ-N04) under an argon atmosphere at room temperature. The samples were sealed inside a 316 stainless-steel (SS) vial with a 40:1 ball (equal number of 10 mm and 6 mm diameter balls) to powder mass ratio and milled for 3 h at a rotational speed of 400 rpm.

Ex-situ powder X-ray diffraction (XRD) data was collected to identify the crystalline materials in each sample. Airtight polymethyl methacrylate (PMMA) covered sample holders were used to avoid oxygen and moisture contamination during data collection. Data were collected using a Bruker D8 Advance Diffractometer (λ = Cu K_α radiation, 40 kV, 40 mA) in the range 10 – 80° 2θ with a 0.03° step size and 1.6 s/step count time. The structural information of each phase was extracted

from the ICDD PDF4 database and the Crystallography Open Database (COD) [22].

In-situ synchrotron radiation X-ray powder diffraction (SR-XRD) was performed at the Australian Synchrotron in Melbourne, Australia [23]. The sample was loaded into a quartz capillary (outer diameter 0.7 mm and wall thickness 0.05 mm) and heated using a hot air blower from room temperature to 900 °C with a 10 °C/min heating rate under dynamic vacuum. Data were acquired using a Mythen microstrip detector (10–40° 2θ) with a 30 s exposure time at two positions, $\lambda = 0.590271(1)$ Å [24]. The temperature of the hot air blower was calibrated against the known thermal expansion coefficient of both NaCl and Ag [25–27].

Temperature programmed desorption-mass spectrometry (TPD-MS) measurements were undertaken using a Stanford Research Systems (SRS, RGA-300) residual gas analyser [28]. Approximately 3 mg of milled CaH_2 was placed in a 316 stainless steel sample holder inside a silicon carbide (SiC, Saint-Gobain) reactor that was connected to the spectrometer using a PTFE gasket to provide an air-tight seal. The samples were heated to 850 °C at 5 °C/min under vacuum ($<7 \times 10^{-4}$ mbar). The corresponding analogue scan of partial pressure *vs* mass to charge ratio was obtained from the RGA software. A K-type thermocouple with an uncertainty of ±1.5 °C was connected inside the SiC tube to record the temperature of the sample.

Thermodynamic properties of the CaH_2 were calculated by performing Pressure Composition Isotherms (PCI), using a computer-controlled Sieverts apparatus [29]. The sample was placed inside a stainless-steel sample holder (without a lid) and then loaded into a silicon carbide (SiC, Saint-Gobain) reactor. H_2 has a negligible hydrogen permeation through SiC and therefore was chosen as the most suitable reactor material for such measurements [29,30]. The sample temperature was measured using a 316 SS K-type thermocouple, which was kept inside the SiC reactor in direct contact with the sample. Hydrogen gas pressure above 1 bar was recorded using a digital pressure transducer (Rosemount 3051S) with a 0.025% span accuracy (0–150 bar). Pressure data measured below 1 bar collected using an Omega PX409 digital pressure transducer with an accuracy of 0.08% of the 1 bar span. PCI measurements of molten CaH_2 were undertaken between 902 and 932 °C with a 1 bar pressure step size and ~24 h equilibration time per step, whereas solid CaH_2 samples were measured between 788 and 807 °C with a 0.5 bar pressure step size and equilibration time per step of ~3 days due to slower kinetics at lower temperature. The reference volume of the instrument was 23.1 cm^3, while the sample side volume was 31.5 cm^3 at room temperature. The uncertainty analysis for determining the thermodynamics from the PCI experiments was carried out using the Orthogonal Distance Regression (ODR) method in ODRPACK 95 using Igor pro [31].

Differential Scanning Calorimetry (DSC) analysis was performed on ball-milled CaH_2 using a Netzsch STA 449 F3 Jupiter analyser equipped with a Pt furnace under an Ar (purity 99.997%) flow of 40 mL/min. Before entering the DSC, the Ar was passed through a Zr filter (heated to 200 °C) to reduce potential oxygen and moisture impurities in the gas stream. Approximately 10 mg of sample was loaded into an Al_2O_3 crucible inside a glove box and sealed with lids containing a pin-hole to allow gas release. The furnace containing the sample was evacuated prior to being placed under an argon flow to remove traces of air. The analysis was carried out under heating rates of 10, 20 and 25 °C/min by heating from 40 °C to 1000 °C. The temperature and thermal sensitivity calibrations were carried out using In, Zn, Al, Ag and Au reference materials for each heating rate to ensure the accuracy of the data. This provides a temperature accuracy of ±0.2 °C, while the balance had an accuracy of ±20 μg. The uncertainty analysis for determining the activation energy from the DSC experiments was carried out using the Orthogonal Distance Regression (ODR) method in ODRPACK 95 using Igor pro [31].

Results and discussion

The XRD pattern of ball-milled CaH_2 is displayed in Fig. 3. It shows that the sample contains minor CaO impurities. The sample may contain both CaO and $Ca(OH)_2$ impurities, but $Ca(OH)_2$ may be amorphous after ball milling. It is clear from *in-situ* SXRD data (Fig. 4) that $Ca(OH)_2$ diffraction peaks can be seen at temperatures above ~100 °C.

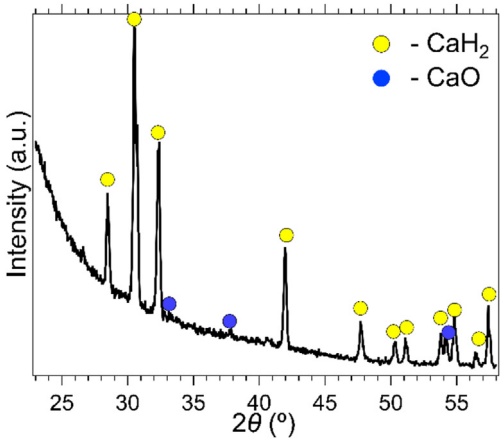

Fig. 3 – *Ex-situ* XRD pattern of ball-milled CaH_2 using (λ = Cu K_α radiation).

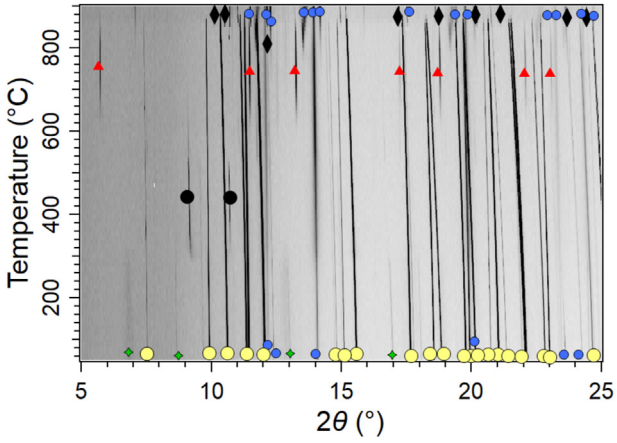

Fig. 4 – *In-situ* SR-XRD pattern of CaH_2 ($\lambda = 0.590271(1)$ Å) with a heating rate of 10 °C/min. Symbols: ● CaH_2, ● CaO, ✦ $Ca(OH)_2$, ● Unknown, ▲ CaH_2·CaO, ♦ Ca.

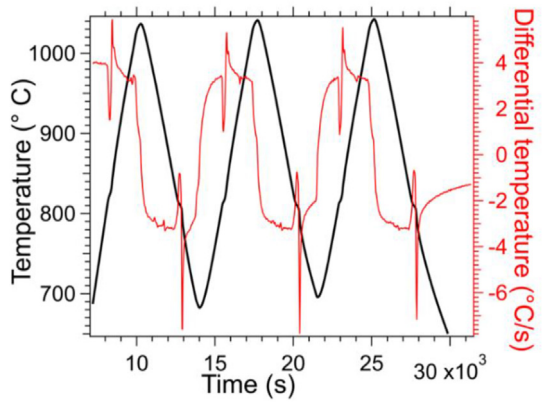

Fig. 5 – Melting point analysis of pure CaH_2 measured inside a Sieverts apparatus under 6 bar H_2. Black line indicates sample temperature and red line is the differential of the temperature. (For interpretation of the references to colour in this figure legend, the reader is referred to the Web version of this article.)

In-situ synchrotron radiation X-ray powder diffraction (SR-XRD) was performed on CaH_2 during a thermal ramp from room temperature to 900 °C as presented in Fig. 4. CaH_2 is present throughout the experiment until it either melts and/or decomposes at ~880 °C when metallic Ca begins to be observed. CaO is present throughout the experiment but does change in intensity throughout the study. As temperature increases, the crystallinity of the $Ca(OH)_2$ impurity increases, although these peaks disappear after 300 °C. Pure $Ca(OH)_2$ has been shown to have an onset of decomposition of ~400 °C [32], although the inclusion of CaH_2 may decrease this temperature. At this point, an unknown crystalline phase with only two identifiable diffraction peaks (2θ = 9.17 and 10.72°) appears and is visible until ~ 700 °C. While the intensity of the unknown phase decreases, another crystalline phase emerges at ~600 °C, and exists until ~830 °C. Six diffraction peaks were identified over the 2θ range of data collected, which allowed for indexing using a cubic space group of $Fd\bar{3}m$ (227:2) with a lattice parameter 10.2271(2) Å. This phase had previously been speculated to be a solid solution of CaH_x [33]. A search for possible isostructural known compounds using the indexed values revealed Ca_2NH as a candidate, which is formed above 900 °C via the reaction between Ca_3N_2 and CaH_2 [34]. Nitrogen is not believed to be present in this sample or experiment due to the vacuum conditions. However, substitution of O into the octahedral N site (16*d*) within the Ca_2NH structure allowed for a clear fit of the indexed peaks and their intensities, indicating that this phase is most probably an oxyhydride, denoted Ca_2OH_2, which can also be described as $CaH_2{\cdot}CaO$. The two H atomic positions in the Ca_2NH structure were originally determined by neutron diffraction to be partially occupied, thus a greater occupancy will also allow for Ca_2OH_2 to be described by the same structure. A range of oxyhydrides have recently been reported with similar structures, where many are formed by thermally treating a metal oxide in the presence of CaH_2 [35,36]. As such, it makes sense that an oxyhydride may also be formed by thermally treating CaH_2 with CaO as performed in Fig. 4. To completely solve the structure of the proposed compound and elucidate the H positions and occupancies, neutron diffraction must be performed. Due to the small X-ray scattering factors of hydrogen atoms, their positions are virtually impossible to determine by powder X-ray diffraction. A sample of CaD_2 containing the oxyhydride phase, measured by powder neutron diffraction, would allow precise location of the H(D) positions and occupancies through Rietveld refinement. Hydrogen is replaced by deuterium for neutron diffraction experiments due to the large incoherent scattering cross section from hydrogen.

Several studies have reported various melting points in the CaH_2 system (800 to $\geq$ 1000 °C), while raw experimental data is also not available in the literature [1]. Hence, the melting point of ball-milled CaH_2 was measured during thermal ramps inside a Sieverts' apparatus while maintaining a hydrogen pressure of 6 bar to minimise the possibility of sample decomposition. Ball-milled CaH_2 (4.4 g) was heated initially from room temperature to 1000 °C and then cooled to 700 °C with a ramp rate of 10 °C/min. The heating and cooling profile were repeated three times between 1000 °C and 700 °C. A sharp thermal signal and discontinuity in the temperature derivative with respect to time was observed at the solidus-liquidus phase transition temperature of 816 ± 7 °C, as shown in Fig. 5.

Fig. 6(a) shows DSC data measured at three heating rates of 10, 20 and 25 °C/min. Each DSC curve shows two endothermic

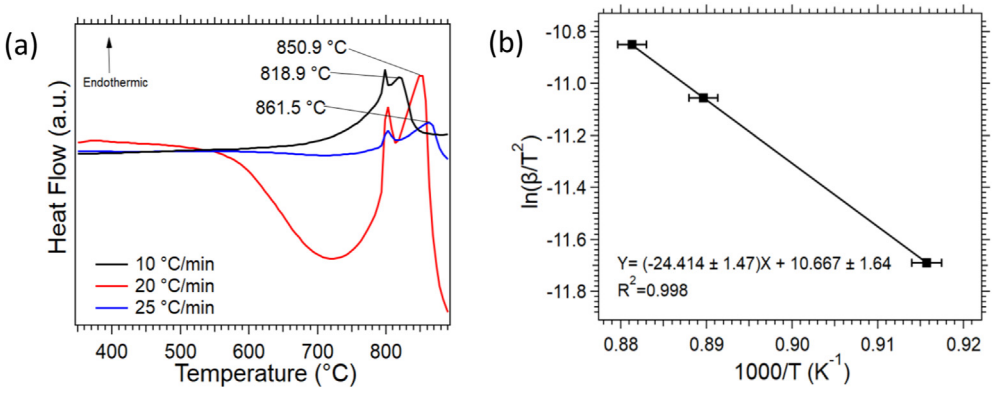

Fig. 6 – (a) Differential scanning calorimetry pattern of CaH_2 measured at 10, 20 and 25 °C. (b) Kissinger plot constructed using the second endothermic peak measured at each heating rate.

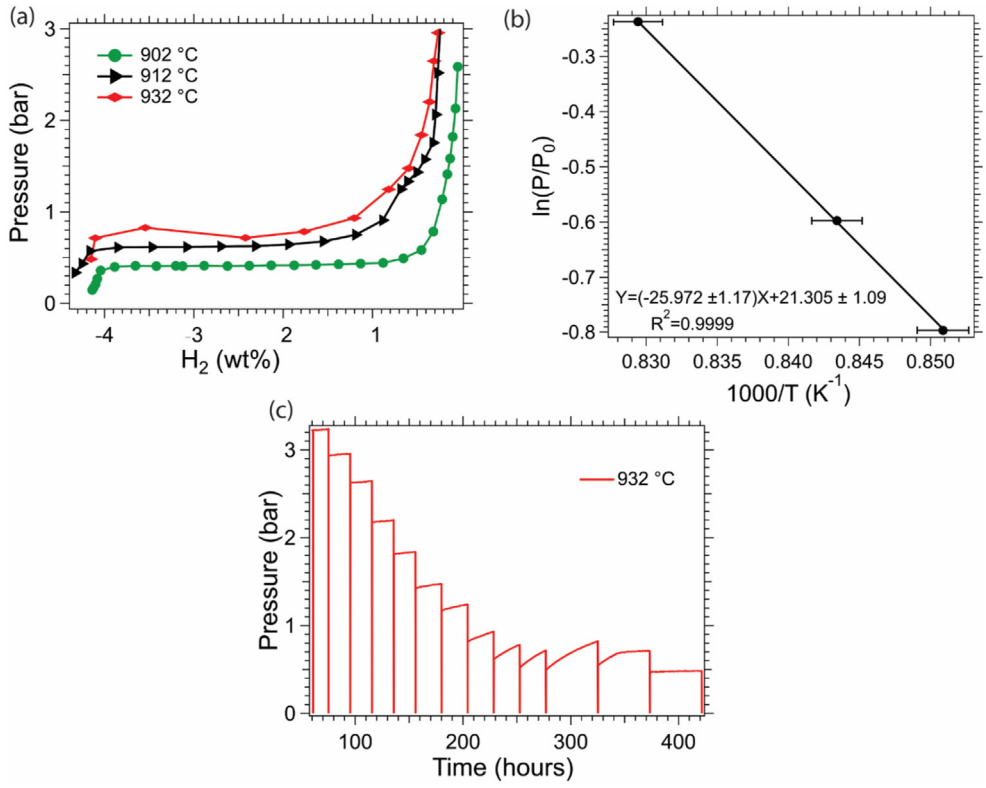

Fig. 7 – (a) PCI's of molten CaH_2 at 902, 912, 932 °C; (b) corresponding van't Hoff plot and (c) raw pressure data at 932 °C.

peaks. The first peak temperature was identical at all heating rates, indicating the solid-liquid phase transition of CaH_2, while the second peak was attributed to the decomposition of CaH_2. The melting point determined by DSC is 802 °C, which is lower than the value of 816 °C obtained from the melting point analysis carried out on the Sieverts' apparatus. Sample contamination may cause a reduction in melting point [37]. In this instance, the melting point reduction may be caused by residual gaseous impurities in the Ar flow causing oxidation, or by slight oxidation of the sample that occurred while transferring the crucible from the glovebox to the DSC instrument. The sample used in the melting point experiment shown in Fig. 5 was never exposed to air as it was loaded in the argon glovebox and sealed. The in situ SR-XRD data could be employed to determine the melting point of CaH_2 as the Bragg peaks for CaH_2 would disappear upon liquefaction. There is a step in the backround at ~830 °C (indicative of a phase change), but some CaH_2 is still apparent in the data after this temperature. This may be attributed to a possible error in the temperature calibration which is not exact and for this reason temperature data is normally used qualitatively.

The peak temperatures of decomposition measured at the three heating rates were used to construct the Kissinger plot illustrated in Fig. 6(b) [38,39]. The activation energy for hydrogen release in the CaH_2 system was calculated as 203 ± 12 kJ mol^{-1}. This is a relatively high value compared to other metal hydrides such as MgH_2 of ~160 kJ mol^{-1} [40]. The increased activation energy explains the slow reaction kinetics observed during the PCI experiments detailed below.

There have not been any experimental thermodynamic data reported in the literature since the 1960's, but those carried out prior to this time show various levels of disagreement in results. In addition, during measurements, none of the investigations separated the thermodynamics of hydrogen release in the CaH_2 system into temperature regimes that considered the liquid and solid states, meaning the temperature ranges for PCI experiments were selected without considering the melting points of both Ca and CaH_2. This could ultimately affect the equilibrium pressure of hydrogen sorption. In this study, the solid to the liquid phase transition of CaH_2 was determined to be 816 °C; as such, thermodynamic measurements were carried out: (1) above the melting point where CaH_2 is in a liquid state; (2) below the melting point, where CaH_2 is solid.

Determining the thermodynamics of desorption for CaH_2 was challenging due to extremely slow kinetics, hence obtaining a complete PCI curve required several weeks. This challenge was amplified when measuring at temperatures below the melting point. In addition, the temperature window only allowed for PCI's to be measured at three temperatures due to the minimum temperature at which hydrogen can be absorbed under measureable kinetics and the upper temperature imposed by the melting point of 816 ± 7 °C, as shown in Fig. 5. The kinetics of hydrogen release improved at higher temperatures, but higher temperatures had other challenges to overcome. At elevated temperature, volatile calcium is also able to evaporate and deposit on cooler parts of the reactor, where it is then at a temperature and pressure suitable for rehydrogenation. Consequently, the full hydrogen capacity (4.79 wt%) was not achieved, especially below the melting point of CaH_2. One other factor that has been observed while studying hydrogen desorption from CaH_2 is a steady increase

of pressure at a constant temperature, as mentioned by Hüttig et al. and Johnson et al. [10,13].

Fig. 7 illustrates (a) the PCI's measured above the melting points of both Ca (842 °C) and CaH_2 (816 °C) and (b) the corresponding van't Hoff plot. The measurements were conducted at 902, 912 and 932 °C. Due to the extremely slow kinetics, the pressure step size varied from one day to over 3 days in an attempt to reach complete desorption, although reaching true thermodynamic equilibrium was unachievable on a realistic timescale (Fig. 7(c)). Despite this, the enthalpy and entropy of hydrogen desorption of molten CaH_2 were determined from the van't Hoff plot in Fig. 7(b), and were calculated as $\Delta H_{des} = 216 \pm 10$ kJ mol^{-1} H_2, $\Delta S_{des} = 177 \pm 9$ J K^{-1} mol^{-1} H_2. As such, the equilibrium desorption temperature (T_{des}) is 947 ± 65 °C at 1 bar H_2 pressure.

Thermodynamic investigations were also conducted at temperatures below the melting points of both Ca and CaH_2, with Fig. 8(a) illustrating the PCI curves measured at 788, 800 and 807 °C. The PCI curves show that the decomposition of the CaH_2 system occurs in two steps, which may have correlations to the exceedingly poor kinetics. Unfortunately, despite several attempts, it was not possible to reach true thermodynamic equilibrium during the PCI curves, and are thus denoted pseudo-PCI curves. This is attributed to the extremely slow reaction kinetics; the waiting time for each step varied from three days to three weeks and was not long enough to complete the full desorption of hydrogen (as shown in Fig. 8(b)). With these kinetics, the complete PCIs may take several years to collect. Despite the non-equilibrium conditions, the van't Hoff plot for the second (lower) plateau region of the PCI curves was constructed (Fig. 8(c)), and corresponding enthalpy and entropy were calculated as $\Delta H_{des} = 172 \pm 12$ kJ mol^{-1} H_2, $\Delta S_{des} = 144 \pm 10$ J K^{-1} mol^{-1} H_2. These thermodynamic values are helpful, despite their non-equilibrium source, to compare with previous literature.

A comparison of the present thermodynamic studies of molten and solid CaH_2 with past studies is presented in Fig. 9. The vertical grey dotted line represents the melting point of CaH_2 and highlights that all, apart from that of Hurd and Walker, were performed across the melting point. The data points measured above the melting point for previous studies of CaH_2 correlate with the values measured in this study for molten CaH_2 (within the uncertainty limit). Moreover, the uncertainty in these numbers may be underestimated as the desorption steps did not reach complete thermodynamic equilibrium despite lengthy waiting periods between steps.

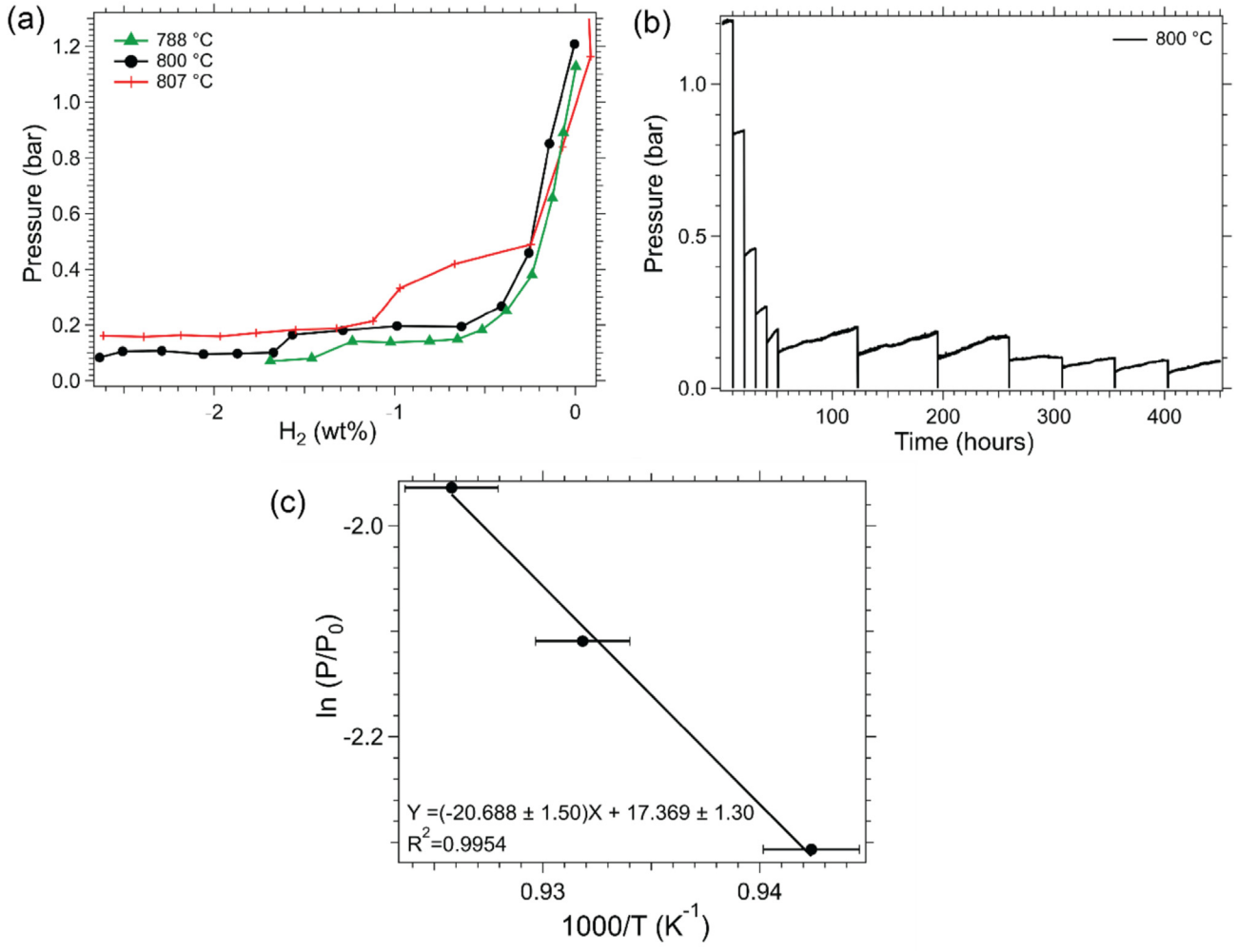

Fig. 8 – (a) Pseudo-PCI's at 788, 800, 807 °C; (b) raw pressure data at 800 °C displaying poor kinetics; and (c) van't Hoff plot of solid CaH_2.

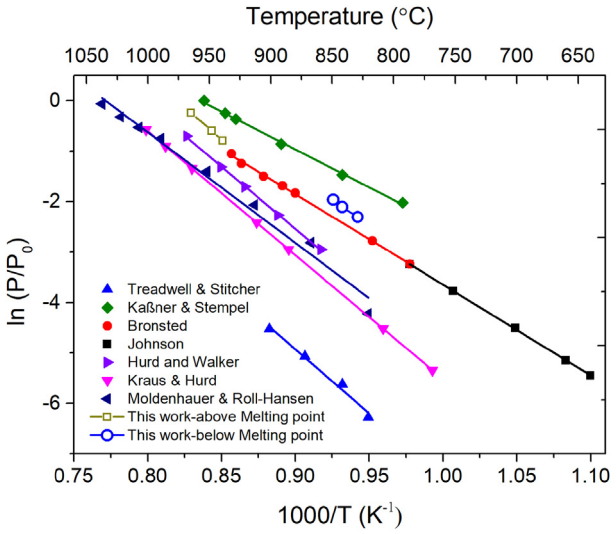

Fig. 9 – Comparison of thermodynamic properties of the present studies with literature works [1,10–19]. The grey hashed line illustrates the melting point of CaH_2.

The thermodynamic values in the literature may also be underestimated, although this is difficult to ascertain as no kinetic pressure data have been previously published. Although, it is clear that PCI step sizes may need to be increased as Curtis et al. explained that 12–16 h steps were used during their experiment for temperatures above 880 °C [7]. Despite the van't Hoff plot for the molten and solid CaH_2 looking potentially linear in this study, the slopes and intercepts are clearly dissimilar as illustrated in Figs. 7 and 8. The y-axis in Fig. 9 is on a logarithmic scale and doesn't allow for the difference to be clearly discerned.

Conclusions

A critical assessment has been made on the previous thermodynamic studies of the CaH_2 system after little research had been carried out since the 1960s. Within these studies, several investigators reported conflicting results and conclusions concerning the thermodynamic properties of the Ca–H system. All thermodynamic studies were completed without considering the melting point of Ca and CaH_2. Hence, the primary purpose of this study was to determine the thermodynamics of both liquid and solid CaH_2 and provide values that can be employed during future studies or technological applications.

A lengthy experimental investigation was performed on the Ca–H system. The melting point of CaH_2 was determined as 816 ± 7 °C using a Sievert's apparatus with hydrogen backpressure. The thermodynamics of CaH_2 above and below this point were then attempted to be determined by PCI analysis. A key discovery was the presence of incredibly slow dehydrogenation reaction kinetics, which were still steadily ongoing after weeks of ongoing measurements. True thermodynamic data obtained from PCI measurements would require years of data collection with these kinetics. As such, pseudo-PCIs were collated to compare our data to previous studies, with estimated thermodynamics of reaction. The thermodynamics of hydrogen release from molten CaH_2 were measured to be ΔH_{des} = 216 ± 10 kJ mol^{-1} H_2, ΔS_{des} = 177 ± 9 J K^{-1} mol^{-1} H_2, providing a 1 bar equilibrium desorption temperature (T_{des}) of 947 ± 65 °C. For solid CaH_2 a ΔH_{des} of 172 ± 12 kJ mol^{-1} H_2, and ΔS_{des} of 144 ± 10 J K^{-1} mol^{-1} H_2 were measured.

The activation energy of the system was calculated from a Kissinger plot as 203 ± 12 kJ mol^{-1}, which is relatively high compared to other metal hydrides. This activation energy explains the extended desorption times required during the PCI experiments, especially at low temperatures. The slow reaction kinetics, the solubility of Ca in CaH_2 and vice versa (formation of condensed mixture phase), allotropic transformations of both Ca and CaH_2, volatile and corrosive nature of Ca and CaH_2, and the high-temperature requirement for a practical working pressure makes the Ca–CaH_2 system complicated and challenging to investigate. Due to the high operating temperatures of 947 ± 65 °C at 1 bar H_2 pressure and energy density of 5131 kJ/kg, this material has been heralded as an ideal thermal energy storage material, but due to the dearth of studies carried out on this material since the 1960's many of these performance issues have not been discussed, until now. Future studies should aim to collect hydrogen pressure data at even higher temperatures (>1000 °C) to promote faster reaction kinetics, which may allow thermodynamic equilibrium to be reached in a reasonable timeframe.

Author contributions

The manuscript was written through contributions of all authors. All authors have approved the final version of the manuscript.

Declaration of competing interest

The authors declare that they have no known competing financial interests or personal relationships that could have appeared to influence the work reported in this paper.

Acknowledgements

CEB, MP and TDH acknowledge the Department of Industry, Science, Energy and Resources for funding from a 2019 Global Innovation Linkage (GIL73589) grant Round 2, and the financial support of the Australian Research Council for ARC Discovery grant DP200102301. The synchrotron powder diffraction data was collected on the Powder Diffraction beamline at the Australian Synchrotron, part of ANSTO.

REFERENCES

[1] Kilb EP. Literature survey on calcium hydride. 1959. APEX485.
[2] Brauer G. Handbook of preparative inorganic chemistry V2. New York: Elsevier, Academic press inc.; 1965.

[3] Wietelmann U, Felderhoff M, Rittmeyer P. Hydrides. https://doi.org/10.1002/14356007.a13_199.pub2. [Accessed 4 January 2023].

[4] Manickam K, Mistry P, Walker G, Grant D, Buckley CE, Humphries TD, et al. Future perspectives of thermal energy storage with metal hydrides. Int J Hydrogen Energy 2019;44:7738–45. https://doi.org/10.1016/j.ijhydene.2018.12.011.

[5] Balakrishnan S, Sofianos MV, Humphries TD, Paskevicius M, Buckley C. Thermochemical energy storage performance of zinc destabilised calcium hydride at high-temperatures. Phys Chem Chem Phys 2020;22:25780–8. https://doi.org/10.1039/D0CP04431H.

[6] Harries DN, Paskevicius M, Sheppard DA, Price TEC, Buckley CE. Concentrating solar thermal heat storage using metal hydrides. Proc IEEE 2012;100:539–49. https://doi.org/10.1109/Jproc.2011.2158509.

[7] Curtis R, Chiotti P. Thermodynamic properties of calcium hydride. J Phys Chem 1963;67:1061–5. https://doi.org/10.1021/j100799a027.

[8] Lide DR. CRC handbook of chemistry and physics. CRC Press; 2004.

[9] Bird JE, Humphries TD, Paskevicius M, Poupin L, Buckley CE. Thermal properties of thermochemical heat storage materials. Phys Chem Chem Phys 2020;22:4617–25. https://doi.org/10.1039/c9cp05940g.

[10] Johnson WC, Stubbs MF, Sidwell AE, Pechukas A. The rate of formation and the dissociation of calcium hydride. J Am Chem Soc 1939;61:318–29. https://doi.org/10.1021/ja01871a026.

[11] Treadwell W, Sticher J, Über den Wasserstoffdruck von Calciumhydrid. Helv Chim Acta 1953;36:1820–32. https://doi.org/10.1002/hlca.19530360720.

[12] Hurd CB, Walker KE. The thermal dissociation of calcium hydride. J Am Chem Soc 1931;53:1681–9. https://doi.org/10.1021/ja01356a008.

[13] Hüttig GF, Brodkorb F. Studien zur Chemie des Wasserstoffes. IV. Zur Kenntnis des Kupferhydrids. Z Anorg Allg Chem 1926;153:235–45. https://doi.org/10.1002/zaac.19261530120.

[14] Ephraim F, Michel E, Metallhydride II Über. Hydride der Erdalkalimetalle und des Lithiums. Helv Chim Acta 1921;4:900–24.

[15] Kaßner G, Stempel B. Über die Aufnahme von Wasserstoff durch Calcium und seine Legierungen. Z Anorg Allg Chem 1929;181:83–94. https://doi.org/10.1002/zaac.19291810107.

[16] Kraus CA, Hurd CB. Equilibria in systems involving calcium, hydrogen and nitrogen. J Am Chem Soc 1923;45:2559–74. https://doi.org/10.1021/ja01664a012.

[17] Moldenhauer W, Roll-Hansen C, Calciumwasserstoff Über. Z Anorg Chem 1913;82:130–40.

[18] Wang M, Sun W, Sha C, Hu B, Du Y, Sun L, et al. Thermodynamic modeling of the Li-H and Ca-H systems. J Phase Equilibria Diffus 2012;33:89–96. https://doi.org/10.1007/s11669-012-9997-z.

[19] Bronsted J. Thermodynamics of calcium hydride formation. Z Elektrochem Angew Phys Chem 1914;20:81–3.

[20] Peterson D, Fattore V. Calcium-calcium hydride phase system. J Phys Chem 1961;65:2062–4. https://doi.org/10.1021/j100828a034.

[21] Wang K, Du J, Kong X, Zeng X, Zou J, Li Z, et al. Ab initio and thermodynamic investigation on the Ca–H system. Int J Hydrogen Energy 2011;36:13632–9. https://doi.org/10.1016/j.ijhydene.2011.08.018.

[22] Gražulis S, Daškevič A, Merkys A, Chateigner D, Lutterotti L, Quiros M, et al. Crystallography Open Database (COD): an open-access collection of crystal structures and platform for world-wide collaboration. Nucleic Acids Res 2011;40:D420–7. https://doi.org/10.1093/nar/gkr900.

[23] Wallwork KS, Kennedy BJ, Wang D. The high resolution powder diffraction beamline for the Australian Synchrotron. AIP Conf Proc 2007;879:879. https://doi.org/10.1063/1.2436201.

[24] Schmitt B, Bronnimann C, Eikenberry EF, Gozzo F, Hormann C, Horisberger R, et al. Mythen detector system. Nucl Instrum Methods A 2003;501:267–72. https://doi.org/10.1016/S0168-9002(02)02045-4.

[25] Pathak P, Vasavada N. Thermal expansion of NaCl, KCl and CsBr by X-ray diffraction and the law of corresponding states. Acta Crystallogr Sect A Cryst Phys Diffr Theor Gen Crystallogr 1970;26:655–8. https://doi.org/10.1107/S0567739470001602.

[26] Hu J, Cai W, Li C, Gan Y, Chen L. In situ x-ray diffraction study of the thermal expansion of silver nanoparticles in ambient air and vacuum. Appl Phys Lett 2005;86:151915. https://doi.org/10.1063/1.1901803.

[27] Hansen BR, Møller KT, Paskevicius M, Dippel A-C, Walter P, Webb CJ, et al. In situ X-ray diffraction environments for high-pressure reactions. J Appl Crystallogr 2015;48:1234–41. https://doi.org/10.1107/S1600576715011735.

[28] Srs RGA. https://www.thinksrs.com/products/vac.html;. [Accessed 4 January 2023].

[29] Sheppard DA, Paskevicius M, Javadian P, Davies IJ, Buckley CE. Methods for accurate high-temperature Sieverts-type hydrogen measurements of metal hydrides. J Alloys Compd 2019;787:1225–37. https://doi.org/10.1016/j.jallcom.2019.02.067.

[30] Alonso JA, Retuerto M, Sanchez-Benitez J, Fernández-Díaz MT. Crystal structure and bond valence of CaH2 from neutron powder diffraction data. Z für Kristallogr - Cryst Mater 2010;225:225–9. https://doi.org/10.1524/zkri.2010.1258.

[31] Boggs PT, Rogers JE. Orthogonal distance regression. Contemp Math 1990;112:183–94.

[32] Khachani M, El Hamidi A, Halim M, Arsalane S. Non-isothermal kinetic and thermodynamic studies of the dehydroxylation process of synthetic calcium hydroxide $Ca(OH)_2$. J Mater Environ Sci 2014;5:615–24.

[33] Griffond ACM, Sofianos MV, Sheppard DA, Humphries TD, Sargent A-L, Dornheim M, et al. High-temperature thermochemical energy storage using metal hydrides: destabilisation of calcium hydride with silicon. J Alloys Compd 2021;858:158229. https://doi.org/10.1016/j.jallcom.2020.158229.

[34] Brice J-F, Motte J-P, Courtois A, Protas J, Aubry J. Etude structurale de Ca2NH par diffraction des rayons X, diffraction des neutrons et résonance magnétique nucléaire du proton dans le solide. J Solid State Chem 1976;17:135–42. https://doi.org/10.1016/0022-4596(76)90213-9.

[35] Beste A, Bufford D. Understanding the $TiH_{(2-x)}/TiO_y$ system at elevated temperature: a literature review. USA: Sandia National Laboratories; 2021.

[36] Valeeva AA, Gusev AI. Placement of H atoms in the crystal lattice of cubic titanium oxyhydride: simulation and diffraction experiment. Mendeleev Commun 2022;32:302–4. https://doi.org/10.1016/j.mencom.2022.05.003.

[37] Brittain C. Using melting point to determine purity of crystalline solids. 2016. https://www.chm.uri.edu/mmcgregor/chm228/use_of_melting_point_apparatus.pdf;. [Accessed 4 January 2023].

[38] Kissinger HE. Reaction kinetics in differential thermal analysis. Anal Chem 1957;29:1702–6. https://doi.org/10.1021/ac60131a045.

[39] Blaine RL, Kissinger HE. Homer kissinger and the kissinger equation. Thermochim Acta 2012;540:1–6. https://doi.org/10.1016/j.tca.2012.04.008.

[40] Yartys VA, Lototskyy MV, Akiba E, Albert R, Antonov VE, Ares JR, et al. Magnesium based materials for hydrogen based energy storage: past, present and future. Int J Hydrogen Energy 2019;44:7809–59. https://doi.org/10.1016/j.ijhydene.2018.12.212.